Applied Surface Science 387 (2016) 109–117

Contents lists available at ScienceDirect

Applied Surface Science

journal homepage: www.elsevier.com/locate/apsusc

Very high frequency plasma reactant for atomic layer deposition

Il-Kwon Oh[a], Gilsang Yoo[a], Chang Mo Yoon[a], Tae Hyung Kim[b], Geun Young Yeom[b], Kangsik Kim[c], Zonghoon Lee[c], Hanearl Jung[a], Chang Wan Lee[a], Hyungjun Kim[a,*], Han-Bo-Ram Lee[d,*]

[a] School of Electrical and Electronic Engineering, Yonsei University, Seoul 120-749, Republic of Korea
[b] Department of Advanced Materials Engineering, Sungkyunkwan University, Suwon 440-746, Republic of Korea
[c] School Materials Science and Engineering, Ulsan National Institute of Science and Technology (UNIST), Ulsan 44919, Korea
[d] Department of Materials Science and Engineering, Incheon National University, 406-840 Incheon, Republic of Korea

ARTICLE INFO

Article history:
Received 11 February 2016
Received in revised form 7 June 2016
Accepted 8 June 2016
Available online 14 June 2016

Keywords:
Very high frequency plasma source
Plasma-enhanced atomic layer deposition
Interlayer-free deposition
High-*k* dielectrics
Damage-free deposition

ABSTRACT

Although plasma-enhanced atomic layer deposition (PE-ALD) results in several benefits in the formation of high-*k* dielectrics, including a low processing temperature and improved film properties compared to conventional thermal ALD, energetic radicals and ions in the plasma cause damage to layer stacks, leading to the deterioration of electrical properties. In this study, the growth characteristics and film properties of PE-ALD Al_2O_3 were investigated using a very-high-frequency (VHF) plasma reactant. Because VHF plasma features a lower electron temperature and higher plasma density than conventional radio frequency (RF) plasma, it has a larger number of less energetic reaction species, such as radicals and ions. VHF PE-ALD Al_2O_3 shows superior physical and electrical properties over RF PE-ALD Al_2O_3, including high growth per cycle, excellent conformality, low roughness, high dielectric constant, low leakage current, and low interface trap density. In addition, interlayer-free Al_2O_3 on Si was achieved in VHF PE-ALD via a significant reduction in plasma damage. VHF PE-ALD will be an essential process to realize nanoscale devices that require precise control of interfaces and electrical properties.

1. Introduction

High-permittivity (high-*k*) dielectrics have been explored as an alternative gate insulator to conventional SiO_2 in metal-oxide-semiconductor-field-effect-transistor (MOSFET) technology [1–3]. Among various high-*k* deposition techniques, atomic layer deposition (ALD) is favored due to its excellent process controllability for extremely thin high-*k* films [4]. Plasma-enhanced ALD (PE-ALD) using plasma reactants has been spotlighted because of several advantages over conventional thermal ALD using gas reactants, such as high growth per cycle (GPC) and a wide process window induced by the high chemical reactivity of plasma radicals in the reactant [5–8]. High-k dielectrics produced via PE-ALD have been widely used for dynamic random access memory (DRAM) capacitor insulators and MOSFET gate dielectrics [9–11].

Some of the plasma sources that generate ions such as the direct plasma and the remote plasma may negatively influence the electrical properties of the high-*k* films in MOSFETs because ion bombardment by the energetic ions can generate defects in the films. For instance, plasma radicals mechanically penetrate films and disrupt chemical stoichiometry, leading to deterioration of the electrical properties of the oxide [12–14]. In addition, the highly energetic plasma radicals usually generate a thick interlayer between the PE-ALD high-k films and Si substrate. Since the formation of an interlayer changes a designed *k* value and affects the electrical properties in the high-*k* stack, the deposition of an interlayer-free high-*k* is desired. Generally, the interlayer in the PE-ALD is thicker than that in thermal ALD, since the energetic species of PE-ALD, such as plasma ions and/or radicals, can react with substrate atoms farther from the surface than those accessible with thermal ALD [15,16]. Researchers have devoted significant effort to minimize the negative effects of plasma on film quality and device properties. In the attempts for a PE-CVD, a pulsed plasma was used in place of the continuous plasma to reduce the ion bombardment period on the surface by shortening the total plasma exposure time [6,17–19]. In other reports, plasma was remotely generated and transferred to the deposition chamber, so that the substrates were less affected by ion bombardment than in the case of direct plasma exposure [20,21].

* Corresponding authors.
E-mail addresses: hyungjun@yonsei.ac.kr (H. Kim), hbrlee@inu.ac.kr (H.-B.-R. Lee).

http://dx.doi.org/10.1016/j.apsusc.2016.06.048
0169-4332/

Very high frequency (VHF) plasma was used in place of the commonly-used 13.56 MHz radio frequency (RF) plasma in the report on plasma-enhanced chemical vapor deposition (PE-CVD) processes [22–25]. The VHF plasma typically has a frequency in the range of 60–150 MHz, so that the plasma density of VHF plasma is higher than that of RF plasma, and the kinetic energy of ions and/or radicals on the surface in VHF plasma is usually lower than that in RF plasma [26]. Compared to RF plasma, the negative effects of plasma-on-film properties are less significant in the VHF plasma process due to its low-ion kinetic energy and high plasma density [26,27]. For amorphous Si deposition, the VHF PE-CVD process shows several advantages over RF PE-CVD, such as high film quality and high growth rate, rendering higher production yield and lower cost [27]. Therefore, VHF plasma is expected to be superior to RF plasma as a reactant for thin film deposition processes in the context of higher GPC and lower ion damage [28–30]. Although a low-damage and interlayer-free PE-ALD process has great importance for industrial purposes as well as scientific understanding, there has been no report on PE-ALD using VHF plasma as well as PE-CVD oxide using VHF plasma so far. Since the key mechanism of CVD growth is quite different to that of ALD growth, the application of VHF plasma to PE-ALD is not simple but the process conditions, such as plasma matching, should be carefully controlled. Furthermore, the conventional thermal ALD and RF PE-ALD have well met the requirements of thin film deposition so far, however, the current real nanodevices fabricated in the range of few nanometers require much better quality and precise control in thin film deposition. Therefore, we employed a new plasma source for novel PE-ALD to achieve high quality dielectric layers for the next generation nanodevices.

For this study, we conducted a comparative study of growth characteristics and film properties by varying plasma process parameters. Al_2O_3 was selected due to its applicability for a wide range of applications, such as a high-*k* dielectric for MOSFET gate oxides [31], a high-density moisture barrier for an organic light emitting diode (OLED) [32], and surface passivation for silicon solar cells [33]. Al_2O_3 films were grown using 13.56 MHz for RF and 60 for VHF PE-ALD with plasma generating powers of 100, 200, and 300 W. The effects on plasma were studied in terms of ALD growth characteristics and film properties such as roughness, density, interlayer thickness, conformality, chemical composition, and electrical properties.

2. Materials and methods

We used a commercial ALD chamber (ALD5008 of SNTEK Co.). The ALD system has a double showerhead for improved uniformity. A plasma matcher controls the variable capacitor to optimize the forward and reflected power, delivering constant power to the process chamber. O_2 plasma of the capacitively-coupled plasma (CCP) type was generated between the showerhead connected to the plasma matcher and the substrate, which was grounded during the reactant exposure step. For PE-ALD, plasma reactant was generated using frequencies of 13.56 MHz and 60 MHz for RF and VHF, respectively. The plasma sources were switchable by changing the cables connecting the matcher and showerhead (see the chamber schematics in Fig. S1 of the Supporting information).

Trimethylaluminum (TMA) and O_2 plasma were used for precursor and oxidant, respectively. The TMA was contained in a stainless steel bubbler and evaporated at room temperature. Ar gas with a flow rate of 50 sccm was used for the purging of excess gas molecules and byproducts between each precursor and reactant exposure step. Growth characteristics of ALD Al_2O_3 on Si substrates were systematically investigated by changing precursor exposure time, O_2 plasma exposure time, purging time, and cycle number to find optimized conditions. Both purging times for precursor and oxidant were kept to 5 s in all of the experiments since GPCs of both RF and VHF PE-ALD Al_2O_3 were saturated over 5 s of purging time (see Fig. S2(e) and (f) of the Supporting information). The substrate temperature was maintained at 180 °C for all ALD processes. To investigate plasma characteristics such as plasma density (N_i) and electron temperature (T_e), a Langmuir probe (Hiden Analytical of ESPION) was installed in the center, 3.5 cm over the substrate. The probe was a cylindrical tungsten wire 0.15 mm in diameter and 10 mm in length. The probe tip was supported by a ceramic tube, which was 1.2 mm in diameter and enclosed by a compensated electrode.

The thickness of the films was measured via spectroscopic ellipsometry (Elli-SE-F of Ellipso Technology). The chemical composition and impurity levels were analyzed via X-ray photoelectron spectroscopy (XPS, AXIS NOVA of KRATOS) with a monochromatic Al Kα source (hv = 1486.7 eV and analysis area: 100 μm^2). The surface C 1 s peak at 285 eV was used as a reference to calibrate the spectrum energy. The film density and roughness of the PE-ALD Al_2O_3 were analyzed using X-ray reflectivity (XRR) with Cu Kα radiation (Smart Lab of Rigaku). An XRR simulation was performed using GlobalFit software. Best-fitted results were obtained using a three-layer-model consisting of PE-ALD Al_2O_3/interfacial layer/Si substrate, instead of a two-layer-model consisting of PE-ALD Al_2O_3/Si substrate. The goodness of the fit values for the RF PE-ALD and the VHF PE-ALD are 0.988 and 0.981, respectively, which are higher than those of other models (see Table S1 in the Supporting information). The surface morphology of the films was analyzed with an atomic force microscope (AFM, Multimode of VEECO). To examine the conformality of PE-ALD Al_2O_3 inside a nanosized 3D structure, SiO_2 hole patterns with diameter and length measurements of 37 nm and 1.5 μm (aspect ratio = 40.5:1), respectively, were prepared. For atomic analysis of the interfacial layer between the substrate and the Al_2O_3 thin-film, we used a JEOL 2100 F electron microscope with a field emission gun operated at accelerating voltages of 200 kV. In this work, the specimens for the transmission electron microscopy (TEM) and scanning TEM (STEM) observations were formed of the thin-film and the trench structure. The thin-film structure specimen was prepared by tripod polishing and low angle ion milling using 1050 TEM mill (E.A. Fischione Instruments) focused by Ar^+ ion thinning. The trench structure specimen preparation was performed by Quanta 3D FIB (FEI) and ion milling using 1040 NanoMill (E.A. Fischione Instruments) focused by Ar^+ ion thinning. The step coverages of RF and VHF Al_2O_3 on the sidewalls of the hole structure were calculated as a reference of the thickness on the top of hole structure.

For metal-oxide-semiconductor (MOS) capacitor fabrication, PE-ALD Al_2O_3 films were deposited on p-type Si substrates. The Si substrates were cleaned at 70 °C for 10 min in SC1 solution ($NH_4OH:H_2O_2:H_2O$ = 1:1:5), followed by dipping in buffered oxide etchant solution for 30 s to remove native oxide. After the oxide deposition, post-deposition annealing (PDA) was carried out via a rapid thermal annealing (RTA) system in N_2 atmosphere at 400 °C for 10 min. Ru was used as the metal electrode of the MOS structure and deposited via DC magnetron sputtering (RSP5003 of SNTEK Co.) with 30 W. The thickness of Ru was 100 nm and a dot-patterned shadow mask with a radius of 100 μm was used to define the contact area. Electrical properties were characterized using a Keithley 590 capacitive-voltage (C-V) analyzer and Agilent 4155C semiconductor parameter analyzer for C-V and current-voltage (I-V) measurements, respectively. The interface trap density (D_{it}) was calculated via a conductance method [34]. The leakage-current densities of a 10-nm-thick Al_2O_3 film were measured at −1 MV/cm. A more detailed description of the electrical evaluation can be found in previous reports [8,35].

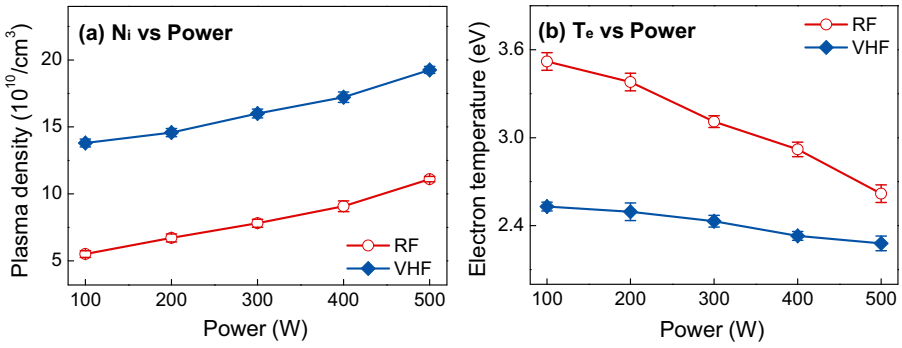

Fig. 1. (a) Plasma density and (b) electron temperature of RF and VHF plasma with increasing plasma power.

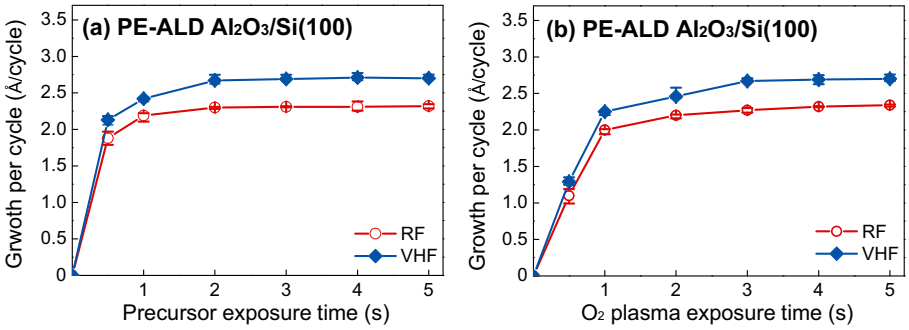

Fig. 2. GPCs of RF and VHF PE-ALD Al_2O_3 on Si with (a) precursor exposure time and (b) O_2 exposure time.

3. Results and discussion

Fig. 1(a) and (b) show the plots of plasma density and electron temperature at various plasma frequencies with increasing plasma power from 100 W to 500 W. As shown in Fig. 1(a), the plasma density increased almost linearly for both frequencies with increasing plasma power. With increasing input power, the electric field between source and substrate was increased due to increased plasma voltage, so that the acceleration of electrons was increased. Therefore, it caused the increase of collision rate leading to increased amount of radicals by the increase of plasma density [36]. In addition, the VHF plasma showed significantly higher plasma density at the same plasma power than the RF plasma. It has been established that higher-frequency plasma, such as VHF plasma, switches the direction of electron acceleration between two electrodes more rapidly than lower-frequency plasma, so that the rate of collision with gas molecules is increased, leading to an increased ionization rate [36,37]. In addition, the potential drop in the sheath region is decreased with increasing power frequency, which increases the plasma power applied to the plasma region resulting in a greater contribution to high plasma density [38].

In contrast to plasma density, electron temperature as a function of plasma power and frequency shows an opposite trend in Fig. 1(b). The RF plasma shows a higher electron temperature than the VHF plasma and the electron temperature decreases on increasing the plasma power for both the RF and the VHF plasma. An electron temperature is followed by below equation [39],

$$V_p - V_f = \frac{KT_e}{2e} ln \frac{\pi m}{2M}$$

where V_p and V_f are the plasma potential and the floating potential, respectively, k is the Boltzmann constant, T_e is electron temperature, m is electron mass, and M is atomic mass. From the equation, the decrease of electron temperature results in the decrease of plasma potential, which is closely related to ion bombardment energy. It might be caused by the decrease in the mean free path of the electron because of the increased electron density in the plasma; i.e., as the electron density increases, the electron mean free path between collisional events decreases. Therefore, an electron loses more of its energy on an average in a high-density plasma than in a low density plasma [40]. A lower electron temperature leads to a lower plasma potential [40], so ions less energetically bombard the surface with a smaller energy. At the same power, therefore, the average ion bombardment energy in the VHF plasma is lower than in the RF plasma

The growth characteristics of PE-ALD Al_2O_3 using the TMA precursor and O_2 plasma were investigated. Fig. 2(a) and (b) show the dependence of the Al_2O_3 GPCs as a function of TMA precursor and O_2 plasma reactant exposure time, respectively. In both cases, the saturation behaviors of GPC were achieved over 2 s and 3 s for the precursor and O_2 plasma reactant exposure time, respectively. The minimum exposure times for saturation are 2 s and 3 s for the precursor and the oxidant, respectively. These times are longer than the reported values[41] because of the relatively large chamber volume rather than the effects of the plasma. The saturated GPC of the VHF plasma was 2.7 Å/cycle, which is higher than the 2.3 Å/cycle of RF plasma PE-ALD. As the ALD is based on self-saturated surface reactions, basically, the GPC should be a function of the substrate species, the reactants, and the substrate temperature. Therefore, for instance, the GPCs should be the same in different chamber configurations with the same substrate, precursor, and temperature. However, PE-ALD can result in higher GPC than conventional thermal ALD [35]. In contrast to conventional thermal ALD in which a requited energy for surface chemical reaction is supplied only by thermal energy form from substrate heating, an additional energy as an electrical energy form from the external electric field is supplied during PE-ALD process. Due to this additional energy from plasma, radicals and ions facilitate the chemical reaction, leading to the improvement of precursor adsorption and nucleation [8]. In addition, electron and ion bombardments during PE-ALD process can also affect the reactions between precursor and oxidant. Thus, these effects from the additional energy result in the increase of

GPC in PE-ALD compared to the conventional thermal ALD. In addition, the GPCs for the RF and VHF plasmas, ~2.2 and ~2.7 Å/cycle, respectively, are higher than the previously reported GPC for the RF PE-ALD Al_2O_3, ~1.2 Å/cycle [41]. This difference can be explained by the effects of the partial pressure of the molecules. As the ALD is based on a surface thermodynamic reaction, the partial pressure of each molecule changes the reaction energy barrier by shifting the chemical equilibria, leading to a change in the GPC [42]. For example, a partial pressure higher by a factor of two for the TMA precursor and the H_2O oxidant resulted in GPCs that were higher by factors of 1.2 and 1.4, respectively [42]. We used 200 sccm of O_2 that is ~3.3 times larger than the amount of O_2 used in previous researches [41] (60 sccm of O_2). In addition, the film thicknesses increased linearly with increasing ALD cycles for both RF and VHF plasma without nucleation incubation (see Fig. S2(a) and (b) of the Supporting information).

Because the same TMA precursor was used for both RF and VHF PE-ALD, the increase in GPC is attributed to the effects of power frequency. An ALD film is grown through a self-saturated reaction, so two effects of the reactant can explain the increase in GPC: an increase in the number of incident oxidant species, and an increase in the reactivity of incident oxidant species. The number of oxidant species is directly related to the plasma density. As shown in Fig. 1(a), the plasma density of VHF plasma is greater than that of RF plasma, a trend similar to that of the GPCs, while the reactivity of the reactants is related to the kinetic energy of radicals and ions, as radicals and ions are the reactive species in the PE-ALD reaction during the oxidant exposure step. Radicals are neutral, so their kinetic energy is not significantly affected by plasma conditions such as plasma power and frequency [43]. In contrast to radicals, the kinetic energy of ions is proportional to electron temperature. The electron temperature of RF plasma is higher than that of VHF plasma in Fig. 1(b), indicating that the reactivity of the reactants in the RF plasma is higher than that in VHF plasma. Since the GPCs of VHF are higher than those of RF, the effect of plasma density is a greater contributor than electron temperature to the increase in GPC. This explanation is consistent with the increase in GPC with increasing plasma power (see Fig. S2 of the Supporting information). Because plasma density increases and electron temperature decreases with increasing plasma power as shown in Fig. 1(a) and (b), the increase in GPC at higher plasma power can be explained only via the dominant contribution of plasma density. The ALD growth based on a self-limiting reaction occurs through two surface reactions during one ALD cycle; one is the adsorption of the precursor on the surface and the other is the oxidation of the precursor adsorbed on the surface by the oxidant. The self-limiting reactions of these two were confirmed, as shown in Fig. 2(a) and (b). Generally, the GPC depends on the density of the adsorbed molecules (both the precursor and the oxidant) under saturation conditions; hence, an increase in the plasma density leads to an increase in the GPC. Thus, a larger number of reaction species in the plasma generates a larger number of adsorption sites for the precursor molecules resulting in an increase in the GPC. Therefore, because the number of the VHF O_2 plasma species is greater than that of the RF O_2 plasma, the GPC of the VHF PE-ALD is higher than that of the RF PE-ALD. Similarly, the increase in the plasma power affects the change of the GPC. As shown in Fig. 1(a), the plasma density increases with an increase in the plasma power, indicating that a higher plasma power generates a larger number of reaction species and adsorption sites, leading to an increase in the GPC. In addition, we continued to observe the saturation behavior of the GPC even at plasma powers up to 300 W (see Fig. S2 of the Supporting information), indicating that the film growth occurred through the ALD reaction, without CVD reactions.

The Al_2O_3 films deposited via RF and VHF plasma for 50 cycles with an RF power of 300 W, and for 55, 46, and 40 cycles with a VHF power of 100, 200, and 300 W, respectively, were analyzed via XRR.

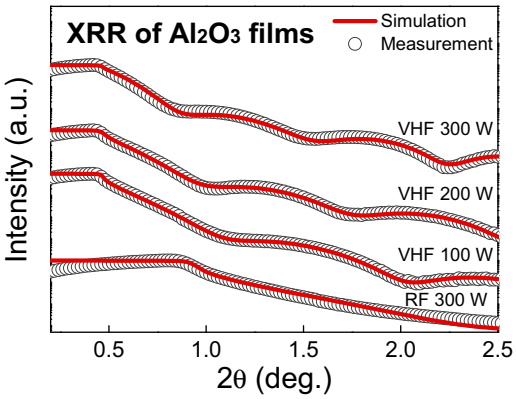

Fig. 3. XRR data and simulation of RF and VHF PE-ALD Al_2O_3 films at various powers.

Table 1
Summary of XRR simulation parameters.

Film properties	VHF			RF
	100 W	200 W	300 W	300 W
Film thickness (nm)	9.30	10.5	11.0	9.20
Interlayer thickness (nm)	0.460	1.21	2.20	3.98
Roughness (nm)	0.140	0.150	0.220	0.400
Film density (g/cm^3)	3.23	3.28	3.35	2.94

In Fig. 3, the measured XRR data was fitted to a simulation model by simultaneously changing the fitting parameters; the obtained physical values of Al_2O_3 film, such as film thickness, interlayer thickness, roughness, and film density, are summarized in Table 1. The best-fit simulation result indicates that an interlayer exists between PE-ALD Al_2O_3 and Si substrate. Based on the reported results, the interlayer is aluminum silicate ($AlSiO_x$), which is commonly observed with Al_2O_3 thin films deposited on Si [44–46]. The composition of the interlayer was confirmed in our EDS analysis and will be discussed in the following section with TEM results.

The Al_2O_3 film thicknesses calculated from the XRR simulation are consistent with thicknesses measured via ellipsometry (see Fig. S2 of the Supporting information for the growth characteristics of VHF and RF PE-ALD Al_2O_3 deposited at various plasma powers). At the same plasma power of 300 W; however, the film densities varied, at 3.35 g/cm^3 for VHF PE-ALD Al_2O_3 and 2.94 g/cm^3 for RF. These values are higher than those of thermal ALD Al_2O_3 with H_2O reactant [47]. Generally, the film density of PE-ALD films is higher than those obtained from thermal ALD due to the densification effect resulting from the momentum transfer of plasma species [48–50]. The radicals and ions accelerated by the external electric field bombard the surface, leading to mechanical densification via momentum transfer [51,52]. The higher density of VHF PE-ALD Al_2O_3 when compared to that of RF can be attributed to higher plasma density. Since VHF plasma has a larger number of radicals and ions which transfer momentum to film, the film density of VHF PE-ALD is higher than that of RF PE-ALD. Although the acceleration of individual particles in RF plasma can be higher than that in VHF plasma due to the higher potential drop in the sheath region, it is likely that the total number of plasma species is a dominant cause of the densification. Similarly, the increase in film density with increasing plasma power can be explained by the increase in plasma density, as shown in Fig. 1(a). The surface roughness obtained via XRR simulation shows the opposite trend in relation to film density. The roughness values were 0.40 nm and 0.22 nm at 300 W for RF and VHF samples, respectively, which is consistent with AFM results (see Fig. S4 of the Supporting information). As mentioned above, the momentum transfer of individual species in RF plasma can be higher than that in VHF plasma, resulting in rough-

Table 2
Summary of film thickness and step coverage measured from TEM images.

Position	RF Al_2O_3		VHF Al_2O_3	
	Thickness (nm)	Step coverage (%)	Thickness (nm)	Step coverage (%)
Top in (b) and (f)	10.3	–	10.4	–
A and D	10.2	99.0	10.4	100
B and E	5.18	50.3	10.1	97.1
C and F	<1	<9.70	9.91	95.4

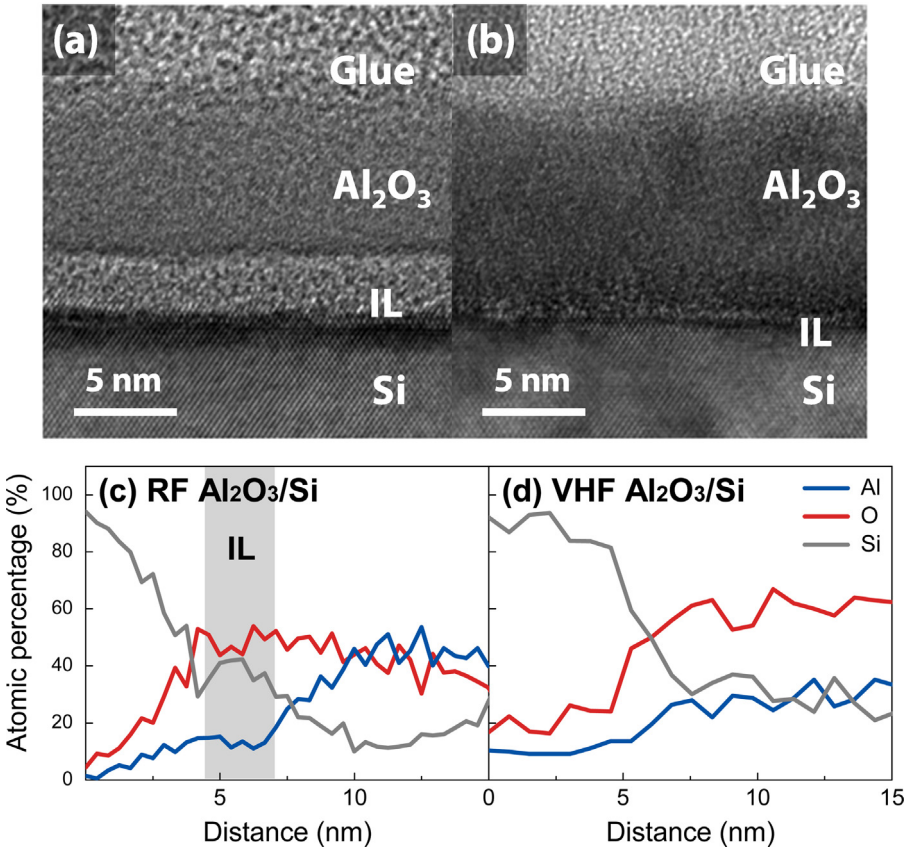

Fig. 4. Cross-sectional TEM micrographs of (a) RF and (b) VHF PE-ALD Al_2O_3 deposited at 100 W of plasma power. EDS line profiles of (c) RF and (d) VHF PE-ALD Al_2O_3.

ening of the film morphology. Interestingly, the thickness of the interfacial layer changed with variations in power frequency and power, similar to the trend of roughness. An interfacial layer can be formed because of three reasons: interdiffusion, inter-reaction, and different film structures at the interface. At a heterojunction interface, the species can interdiffuse into materials owing to a concentration gradient, resulting in the formation of an interfacial layer [53]. In addition, the different species at the interface can with react with each other owing to different thermal stabilities, resulting in an interfacial layer formation [54]. The different film structures can also affect the formation of an interfacial layer because an amorphous phase is thermodynamically more stable than a crystalline phase, hence, they try to form a mixed structure to lower the formation enthalpy. In this case, the film materials and the deposition temperature are the same; hence, other effects contribute to the change in the interlayer thickness including the bombardment effects on the surface during the initial growth. The changes in interlayer thickness will be discussed with visible STEM results in the following paragraph.

Fig. 4(a) and (b) show cross-sectional TEM images of the RF and VHF PE-ALD Al_2O_3, respectively, deposited with 100 W of plasma power, and Fig. 4(c) and (d) are corresponding EDS profiles. The Al_2O_3 films were deposited for 69 and 62 cycles by RF PE-ALD and VHF PE-ALD, respectively. The thicknesses of the RF and VHF PE-ALD Al_2O_3 are 10.3 and 9.8 nm, respectively, which are comparable to XRR thicknesses. As expected from the XRR data above, the interlayer thickness of the VHF PE-ALD Al_2O_3 is significantly smaller than that of the RF PE-ALD films. The measured interlayer thicknesses are approximately 2.9 nm for the RF sample and 0.5 nm for the VHF sample, respectively. Additionally, the existence of an interlayer in the RF PE-ALD Al_2O_3 was clearly observed in the EDS profile in Fig. 4(c). As shown in Fig. 4(c), for the RF sample, the Si signals decrease and then rapidly increase, indicating that a Si diffusion has occurred from the substrate to the interlayer. In contrast, a smooth decrease in the Si signal is observed in Fig. 4(d) for the VHF sample. As mentioned earlier, it is known that the interlayer observed between the Al_2O_3 film and Si substrate is composed of $AlSiO_x$, which is consistent with our EDS results.

The thickness of the interlayer changed with variations in the power frequency and power. As mentioned above, although the number of ions in the VHF plasma is greater than in the RF plasma, the energy of individual ions in the RF plasma is larger than in VHF plasma. Therefore, the ions in the RF plasma penetrate deeper into the Si substrate than those in the VHF plasma, so the O atom can

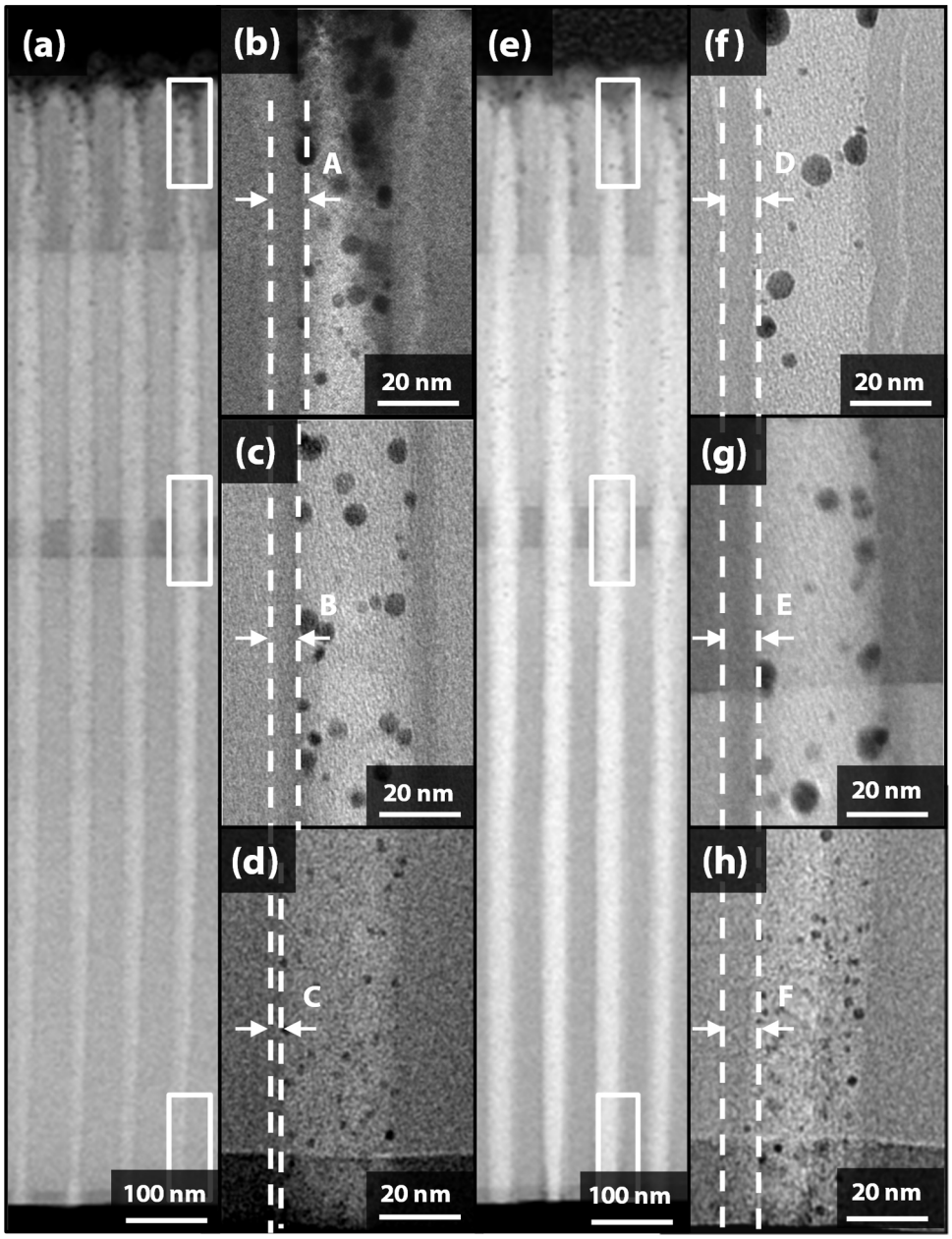

Fig. 5. Cross-sectional TEM images of (a–d) RF and (e–h) VHF Al_2O_3 deposited on SiO_2 nanoholes (40.5:1 of aspect ratio). The hole diameter and depth are 37 nm and 1.5 μm, respectively. Magnified TEM image of RF PE-ALD Al_2O_3 at (b) top, (c) middle, and (d) bottom. Magnified TEM image of VHF PE-ALD Al_2O_3 at (e) top, (g) middle, and (h) bottom.

diffuse in a wider range, resulting in the formation of a thicker interlayer. The increase in interlayer thickness with increasing plasma power in the VHF plasma in Table 1 can be explained by potential drops in the sheath region. The width of the sheath region in plasma is increased with increasing plasma power, so the potential drop in the sheath region is increased. Since the potential drop across the sheath region accelerates ions to the substrate, the ion penetrates deeper into the substrate at the higher plasma power [55], leading to the formation of a thicker interlayer. The interlayer formation during the PE-ALD process is primarily affected by interactions between energetic ions and the substrate. Therefore, the interlayer formation can be correlated with the Si substrate damage. The VHF PE-ALD Al_2O_3 has an ultra-thin interlayer due to generation of a greater number of low-energy ions, so less damage to the Si substrate can be expected when compared to RF plasma.

Excellent conformality inside 3D nanostructures is one of the advantages of ALD. In many cases, however, PE-ALD showed limited conformality compared to thermal ALD [54]. Because radicals and ions are easily recombined inside a 3D nanostructure through collision with the wall, they cannot reach the bottom of the structures while maintaining high chemical reactivity [56,57]. TEM images of the RF and VHF PE-ALD Al_2O_3 showing hole structures are presented in Fig. 5(a) and (e), respectively, and measured thickness and step coverages are summarized in Table 2. As the patterns used for the conformality test had a significant aspect ratio, the patterns were reinforced by depositing additional materials; Ru was deposited by PE-ALD and Pt layers were also deposited using the FIB tool. During the FIB ion milling process, however, the Pt layer was sputtered and re-deposited by the Ga+ ion on the sides of the samples, leading to the formation of Pt nanoparticles, indicated as dark spots in the TEM images. Compared to RF PE-ALD Al_2O_3, VHF PE-ALD Al_2O_3 shows nearly constant step coverages at various positions. In contrast to VHF PE-ALD, the thicknesses of RF PE-ALD Al_2O_3 significantly decreases at the middle and bottom, and the

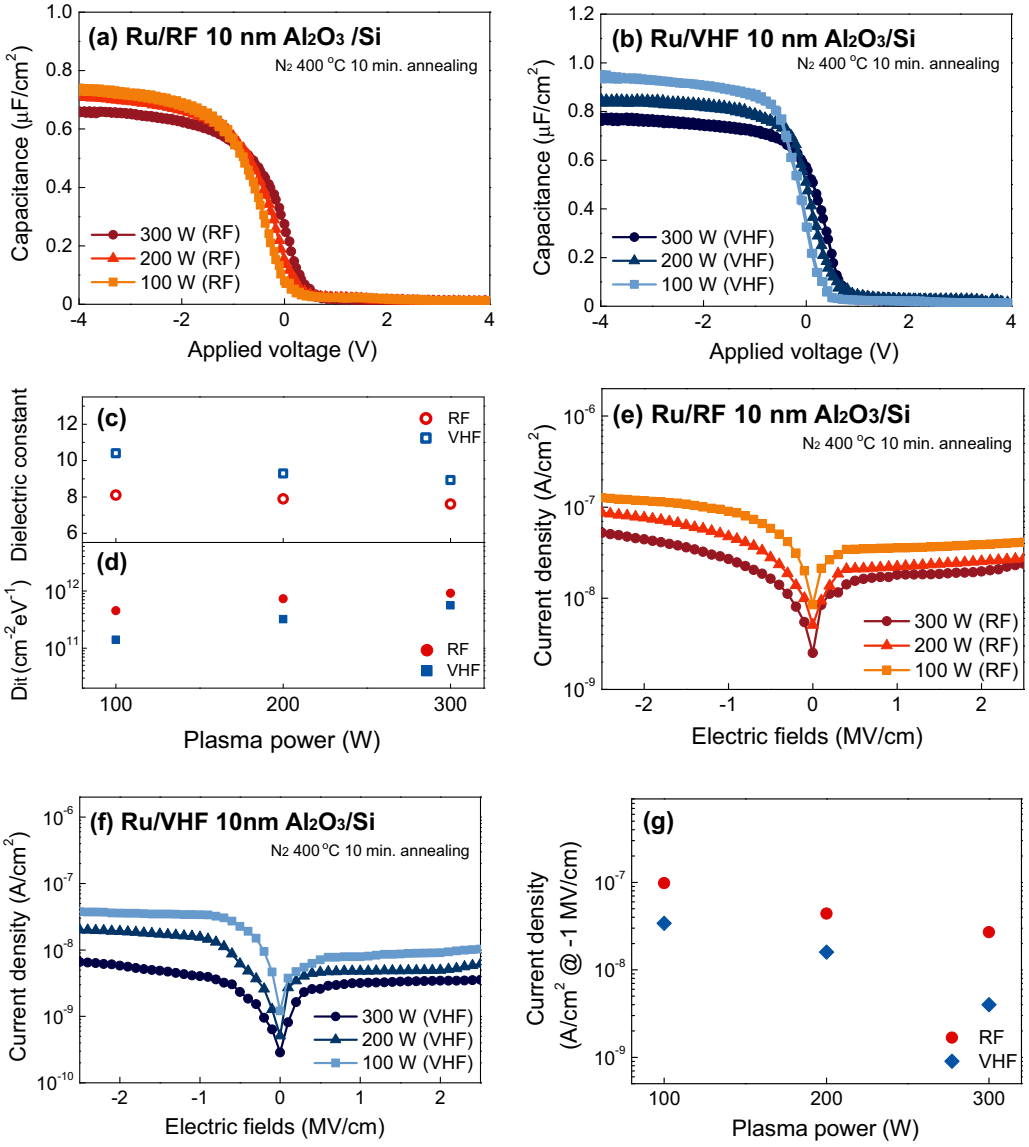

Fig. 6. The C-V curves of MOS capacitors using (a) RF and (b) VHF PE-ALD Al_2O_3 after post-deposition annealing at 400 °C. (c) Dielectric constants and (d) interface trap densities of Al_2O_3 using RF and VHF plasma as a function of plasma power. The I-V curves of MOS capacitors using (e) RF plasma, (f) VHF plasma, and (g) leakage current density at −1 MV/cm using PE-ALD Al_2O_3 with post-deposition annealing at 400 °C.

resulting step coverages are 50.3% and <9.7%, respectively, which are significantly smaller than that of VHF PE-ALD Al_2O_3 at 95.3%. Because the VHF plasma has a higher plasma density than the RF plasma, the probability that the radicals and ions survive to the bottom of the holes is higher in the VHF plasma than in the RF plasma, although the recombination reaction of the plasma species is independent of the plasma source. Therefore, in VHF plasma, a uniform ALD reaction occurs at all of the positions in the holes, resulting in the formation of conformal film.

Fig. 6(a) and (b) show C-V measurement results of RF and VHF PE-ALD Al_2O_3 films at various plasma powers, respectively. Negligible hysteresis of C-V curves was observed in both sweep directions from positive/negative voltage to negative/positive voltage. The dielectric constants of RF and VHF PE-ALD Al_2O_3 were extracted from the maximum capacitance value at −4 V in C-V graphs, and are plotted in Fig. 6(c). All of the dielectric constants of RF PE-ALD Al_2O_3 were found to be smaller than those of VHF PE-ALD Al_2O_3, and decreased with increasing plasma power. The higher constants of VHF PE-ALD Al_2O_3 over those of RF PE-ALD Al_2O_3 are due to the various thicknesses of the $AlSiO_x$ interlayer. Generally, it is known that the $AlSiO_x$ interlayer has a lower dielectric constant than Al_2O_3, and in fact, the dielectric constant of the $AlSiO_x$ interlayer calculated using the thickness measured from TEM images was approximately 4–5, which is smaller than that of Al_2O_3. Because VHF PE-ALD Al_2O_3 has a significantly thinner interlayer than RF PE-ALD Al_2O_3, and the capacitance measured from the C-V analysis is a total capacitance from the series connection of Al_2O_3 and $AlSiO_x$ layers the resulting dielectric constant of VHF PE-ALD Al_2O_3 is larger than that of RF PE-ALD Al_2O_3. Similarly, the change in dielectric constant with increasing plasma power can be explained by the change in interlayer thickness. When the plasma power increased, the dielectric constants decreased in both RF and VHF PE-ALD Al_2O_3 as shown in Fig. 6(c). Because the interlayer thickness increases with increasing plasma power, as shown in Table 1, and the dielectric constant of the interlayer is smaller than that of Al_2O_3, the calculated dielectric constant apparently decreased. The D_{it} values of the RF and VHF samples extracted from the C-V graph are plotted at various plasma powers in Fig. 6(d). The D_{it} values of the VHF samples are lower than those of the RF samples in all of the powers studied. As the electron temperature is related to the plasma potential that

determines the average ion energy, [40] a low electron temperature can be translated to a low ion energy. There are two factors of ion bombardment affecting growth characteristics of Al_2O_3 in plasma generation: the bombardment energy of each ion and the rate of ion bombardment. In terms of film growth, compared to RF plasma, VHF plasma results in the higher GPC with higher plasma density. Higher rate of ion bombardment by higher plasma density in VHF could make higher GPCs than that in RF. In contrast, in terms of substrate damage, there exists the energy barrier to induce the damage on the substrate during ion bombardment, since Al_2O_3 by VHF shows lower plasma damage than that by RF in spite of higher plasma density. In other words, in spite of higher ion bombardment rate due to higher plasma density in VHF plasma, lower energy of ion bombardment results in lower damage of the substrate surface, finally leading to lower interface trap density between Al_2O_3 and Si. In addition, the D_{it} was increased with increasing plasma power. When the plasma power is increased, the potential drop in the sheath region also increases [55], so the ion bombardment energy is increased, resulting in increase of damage relating with D_{it}.

The leakage current densities of MOS capacitors are presented in Fig. 6(e) for RF plasma and (f) for VHF plasma as a function of the plasma power of Al_2O_3 thin films, and are summarized in (g). At all of the powers studied, the leakage currents of RF PE-ALD Al_2O_3 film are larger than those of VHF PE-ALD Al_2O_3. The chemical composition and impurity levels nearly match those in VHF and RF PE-ALD Al_2O_3, except the amount of O—H bonding in the XPS analysis (see Fig. S5 of the Supporting information). The O—H bonding in Al_2O_3 becomes a leakage path [45]. In addition, O—H bonding can be generated in the Al_2O_3 film from residual Al—OH bonds at the surface as a result of incomplete reaction via TMA exposure [58]. Because the plasma density of VHF plasma is higher than that of RF plasma, the VHF plasma more effectively oxidizes the TMA precursor adsorbed on the surface; therefore, less O—H bonding is formed in VHF PE-ALD Al_2O_3 films than in RF PE-ALD Al_2O_3 films, leading to low leakage current. Additionally, oxygen vacancy is another factor for the different I-V characteristics. The oxygen vacancies in the film generate the gap states in E_g that contribute to the leakage current by trap-assisted tunneling [59]. On increasing the plasma power and the power frequency, the stoichiometry of the films reach an ideal ratio of 1.5 in both the cases (see Fig. S5(h) of the Supporting information), indicating that the oxygen vacancies decrease with an increase in the plasma power and the power frequency. Thus, lower leakage currents were observed for the samples at a higher power and frequency. In addition, a decrease in leakage currents was observed in both RF and VHF plasma with increasing plasma power. Since the plasma density increases with increasing plasma power, the larger amounts of plasma species at higher plasma power sufficiently oxidized a greater number of adsorbed TMA precursors than those at the lower plasma power, resulting in the reduction of leakage current. Similarly, an improvement in insulating properties with increasing plasma power was reported several times in PE-ALD Al_2O_3 [55,60] and TiO_2 [61] systems as a result of increased O_2 plasma power.

Due to the higher plasma density and lower electron temperature of VHF plasma compared to RF plasma, VHF PE-ALD has advantages in growth characteristics and electrical properties, such as GPC, film density, interlayer thickness, roughness, conformality, purity, D_{it}, and leakage currents. High plasma density leads to an increase in the number of reactants participating in the ALD reaction, in turn leading to high GPC, film density, and conformality, and low purity and leakage currents. Low electron temperature leads to a reduction in plasma damage to the substrate and film, resulting in almost no interlayer formation, low roughness, high dielectric constant, and low D_{it}. We believe that PE-ALD using VHF plasma reactant will be practically significant for the fabrication of high k layers in nanoscale 3D semiconductor devices that require precise control of interfaces and electrical properties.

4. Conclusions

In summary, the growth characteristics and film properties of PE-ALD Al_2O_3 using RF and VHF plasma reactant were systematically investigated. Compared to RF plasma, VHF plasma significantly reduced plasma damage due to its lower electron temperature. Low-energy ions in the VHF plasma effectively reduce the negative effect of ion bombardment on the Si substrate, so that the resulting PE-ALD Al_2O_3 films have beneficial dielectric properties such as interlayer-free PE-ALD, high dielectric constant, low roughness, and low interface trap charges. Additionally, the high plasma density of VHF plasma positively affects the growth characteristics and film properties of PE-ALD Al_2O_3. Due to an increased number of ions and radicals which are reactive species during ALD reactions, VHF PE-ALD Al_2O_3 shows a high GPC, excellent conformality, high film density, low impurity level, and low leakage currents. VHF PE-ALD is expected to be an alternative to the conventional RF PE-ALD for fabrication of dielectric layers for nanoscale devices that require precise control of interfaces and electrical properties.

Author contributions

The manuscript was written through contributions of all authors. All authors have given approval to the final version of the manuscript.

Acknowledgments

This work was supported by the Industrial Strategic Technology Development Program (10041926, Development of high-density plasma technologies for thin-film deposition of nanoscale semiconductors and flexible display processing) funded by the Ministry of Knowledge Economy (MKE, Korea) and by the MOTIE (Ministry of Trade, Industry & Energy (10053098)) and KSRC (Korea Semiconductor Research Consortium) support program for the development of future semiconductor devices.

Appendix A. Supplementary data

Supplementary data associated with this article can be found, in the online version, at http://dx.doi.org/10.1016/j.apsusc.2016.06.048.

References

[1] D.A. Buchanan, Scaling the gate dielectric: materials, integration, and reliability, IBM J. Res. Develop. 43 (1999) 245–264.
[2] E.P. Gusev, Defects in SiO_2 and Related Dielectrics: Science and Technology, Springer, Netherlands, 2000.
[3] M.L. Green, E.P. Gusev, R. Degraeve, E.L. Garfunkel, Ultrathin (<4 nm) SiO_2 and Si-O-N gate dielectric layers for silicon microelectronics: understanding the processing, structure, and physical and electrical limits, J. Appl. Phys. 90 (2001) 2057.
[4] H. Kim, Atomic layer deposition of metal and nitride thin films: current research efforts and applications for semiconductor device processing, J. Vac. Sci. Technol. B 21 (2003) 2231.
[5] H. Kim, C. Cabral, C. Lavoie, S.M. Rossnagel, Diffusion barrier properties of transition metal thin films grown by plasma-enhanced atomic-layer deposition, J. Vac. Sci. Technol. B 20 (2002) 1321.
[6] M. Seman, J.J. Robbins, S. Agarwal, C. Wolden, Self-limiting growth of tantalum oxide thin films by pulsed plasma-enhanced chemical vapor deposition, Appl. Phys. Lett. 90 (2007) 131504.
[7] C. Detavernier, J. Dendooven, D. Deduytsche, J. Musschoot, Thermal versus plasma-enhanced ALD: growth kinetics and conformality, ECS Trans. 16 (2008) 239.
[8] H. Kim, I.-K. Oh, Review of plasma-enhanced atomic layer deposition: technical enabler of nanoscale device fabrication, Jpn. J. Appl. Phys. 53 (2014) 03DA01.

[9] A.I. Kingon, J.-P. Maria, S. Streiffer, Alternative dielectrics to silicon dioxide for memory and logic devices, Nature 406 (2000) 1032.
[10] O. Sneh, R.B. Clark-Phelps, A.R. Londergan, J. Winkler, T.E. Seidel, Thin film atomic layer deposition equipment for semiconductor processing, Thin Solid Films 402 (2002) 248.
[11] S.-H.K. Park, J. Oh, C.-S. Hwang, J.-I. Lee, Y.S. Yang, H.Y. Chu, Ultrathin film encapsulation of an OLED by ALD, Electrochem. Solid State Lett. 8 (2005) H21.
[12] S. Bothra, C.T. Gabriel, S. Lassig, D. Pirkle, Control of plasma damage to gate oxide during high density plasma chemical vapor deposition, J. Electrochem. Soc. 142 (1995) L208.
[13] K.P. Cheung, C. Pai, Charging damage from plasma enhanced TEOS deposition, Electron Device Lett. IEEE 16 (1995) 220.
[14] S.J. Fonash, Plasma processing damage in etching and deposition, IBM J. Res. Dev. 43 (1999) 103.
[15] A. Callegari, E. Cartier, M. Gribelyuk, H. Okorn-Schmidt, T. Zabel, Physical and electrical characterization of Hafnium oxide and Hafnium silicate sputtered films, J. Appl. Phys. 90 (2001) 6466.
[16] P.K. Park, Roh J.-S, B.H. Choi, S.-W. Kang, Interfacial layer properties of HfO_2 films formed by plasma-enhanced atomic layer deposition on silicon, Electrochem. Solid State Lett. 9 (2006) F34.
[17] H.G. Pryce Lewis, D.J. Edell, K.K. Gleason, Pulsed-PECVD films from hexamethylcyclotrisiloxane for use as insulating biomaterials, Chem. Mater. 12 (2000) 3488.
[18] E.J. Winder, K.K. Gleason, Growth and characterization of fluorocarbon thin films grown from trifluoromethane (CHF_3) using pulsed-plasma enhanced CVD, J. Appl. Polym. Sci. 78 (2000) 842.
[19] S.F. Szymanski, M.T. Seman, C.A. Wolden, Plasma and gas-phase characterization of a pulsed plasma-enhanced chemical vapor deposition system engineered for self-limiting growth of aluminum oxide thin films, Surf. Coat. Technol. 201 (2007) 8991.
[20] G. Lucovsky, D. Tsu, Plasma enhanced chemical vapor deposition: differences between direct and remote plasma excitation, J. Vac. Sci. Technol. A 5 (1987) 2231.
[21] H.B. Profijt, P.M. Kudlacek, C.M. van de Sanden, W.M.M. Kessels, Ion and photon surface interaction during remote plasma ALD of metal oxides, J. Electrochem. Soc. 158 (2011) G88.
[22] T. Nishimoto, M. Takai, H. Miyahara, M. Kondo, A. Matsuda, Amorphous silicon solar cells deposited at high growth rate, J. Non-Cryst. Solids 299 (2002) 1116.
[23] H. Takatsuka, M. Noda, Y. Yonekura, Y. Takeuchi, Y. Yamauchi, Development of high efficiency large area silicon thin film modules using VHF-PECVD, Solar Energy 77 (2004) 951.
[24] S.Y. Myong, K. Sriprapha, Y. Yashiki, S. Miyajima, A. Yamadab, M. Konagai, Silicon-based thin-film solar cells fabricated near the phase boundary by VHF PECVD technique, Sol. Energy Mater. Sol. Cells 92 (2008) 639.
[25] Y. Nakano, S. Goya, T. Watanabe, N. Yamashita, Y. Yonekur, High-deposition-rate of microcrystalline silicon solar cell by using VHF PECVD, Thin Solid Films 506 (2006) 33.
[26] A.I. Kosarev, A.S. Smirnov, A.S. Abramov, A.J. Vinogradov, A. Yu Ustavschikov, M.V. Shutov, Effect of ion bombardment in very-high frequency glow discharge on growth and properties of SiH_x films, J. Vac. Sci. Technol. A 15 (1997) 298.
[27] H. Takatsuka, M. Noda, Y. Yonekura, Y. Takeuchi, Y. Yamauchi, Development of high efficiency large area silicon thin film modules using VHF-PECVD, Sol. Energy 77 (2004) 951.
[28] Y. Mori, K. Yoshii, H. Kakiuchi, K. Yasutake, Atmospheric pressure plasma chemical vapor deposition system for high-rate deposition of functional materials, Rev. Sci. Instrum. 71 (2000) 3173.
[29] M. Matsumoto, M. Shima, S. Okamoto, K. Murata, M. Tanaka, S. Kiyama, H. Kakiuchi, K. Yasutake, K. Yoshii, K. Endo, Y. Mori, Extremely high-rate deposition of silicon thin films prepared by atmospheric plasma CVD method with a rotary electrode, Proceeding of 3rd World Conference on Photovoltaic Energy Conversion (2003) 1552.
[30] H. Hamidinezhad, Y. Wahab, Z. Othaman, Ultra-sharp pointed tip Si nanowires produced by very high frequency plasma enhanced chemical vapor deposition via VLS mechanism, J. Mater. Sci. 46 (2011) 5085.
[31] P. Carcia, R. McLean, M. Reilly, M. Groner, S. George, Ca test of Al_2O_3 gas diffusion barriers grown by atomic layer deposition on polymers, Appl. Phys. Lett. 89 (2006) 031915.
[32] E. Langereis, M. Creatore, S. Heil, M. Van de Sanden, W. Kessels, Plasma-assisted atomic layer deposition of Al_2O_3 moisture permeation barriers on polymers, Appl. Phys. Lett. 89 (2006) 081915.
[33] B. Hoex, S. Heil, E. Langereis, M. Van de Sanden, W. Kessels, Ultralow surface recombination of c-Si substrates passivated by plasma-assisted atomic layer deposited Al_2O_3, Appl. Phys. Lett. 89 (2006) 042112.
[34] D. Park, H. Cho, K. Lim, C. Lim, I. Yeo, J. Roh, J. Park, Characteristics of n^+ polycrystalline-Si/Al_2O_3/Si metal-oxide-semiconductor structures prepared by atomic layer chemical vapor deposition using $Al(CH_3)_3$ and H_2O vapor, J. Appl. Phys. 89 (2001) 6275.
[35] W.-H. Kim, W.J. Maeng, K.-J. Moon, J.-M. Myoung, H. Kim, Growth characteristics and electrical properties of La_2O_3 gate oxides grown by thermal and plasma-enhanced atomic layer deposition, Thin Solid Films 519 (2010) 362–366.
[36] T.H. Kim, K.N. Kim, A.K. Mishra, J.S. Seo, H.B. Jeong, J.O. Bae, G. Yeom, Plasma characteristics of inductively coupled plasma using dual-frequency antennas, Jpn. J. Appl. Phys. 52 (2013) 05EA02.
[37] K. Bera, D. Hoffman, S. Shannon, G. Delgadino, Y. Ye, Frequency optimization for capacitively coupled plasma source, IEEE Trans. Plasma Sci. 33 (2005) 2.
[38] A. Pateau, A. Rhallabi, M.-C. Fernandez, M. Boufnichel, F. Roqueta, Modeling of inductively coupled plasma $SF_6/O_2/Ar$ plasma discharge: effect of O_2 on the plasma kinetic properties, J. Vac. Sci. Technol. A 32 (2014) 021303.
[39] A. Mishara, M.H. Jeon, K.N. Kim, G.Y. Yeom, An investigation of the temporal evolution of plasma potential in a 60 MHz/2 MHz pulsed dual-frequency capacitively coupled discharge, Plasma Sources Sci. Technol. 21 (2012) 055006.
[40] X.-M. Zhu, W.-C. Chen, S. Zhang, Z.-G. Guo, D.-W. Hu, Y.-K. Pu, Electron density and ion energy dependence on driving frequency in capacitively coupled argon plasmas, J. Phys. D: Appl. Phys. 40 (2007) 7019–7023.
[41] J.L. van Hemmen, S.B.S. Heil, J.H. Klootwijk, F. Roozeboom, C.J. Hodson, M.C.M. van de Sanden, W.M.M. Kessels, Plasma and thermal ALD of Al_2O_3 in a commercial 200 mm ALD reactor, J. Electrochem. Soc. 154 (2007) G165.
[42] R. Kuse, M. Kundu, T. Yasuda, N. Miyata, A. Toriumi, Effect of precursor concentration in atomic layer deposition of Al_2O_3, J. Appl. Phys. 94 (2003) 6411.
[43] N. Inagaki, Plasma Surface Modification and Plasma Polymerization, vol. 3, CRC Press, 1996, pp. 265.
[44] J. Park, G.Y. Kim, G. Yeom, Effect of bias frequency variation on the characteristics of SiO_x thin films deposited by atmospheric pressure chemical vapor deposition using a double discharge, Thin Solid Films 539 (2013) 12.
[45] A. Coban, E. Khawaja, S. Durrani, Difference between bulk and thin film densities of metal oxide and fluoride films studied by NRA depth profiling techniques, Nucl. Instrum. Methods Phys. Res. Sect. B 194 (2002) 171.
[46] Z. Qiao, R. Latz, D. Mergel, Thickness dependence of In_2O_3: Sn film growth, Thin Solid Films 466 (2004) 250.
[47] M. Groner, F. Fabreguette, J. Elam, S. George, Low-temperature Al_2O_3 atomic layer deposition, Chem. Mater. 16 (2004) 639.
[48] H. Kim, I. Chung, S. Kim, S. Shin, W. Jung, R. Hwang, C. Jeong, H. Hwang, Improved film quality of plasma enhanced atomic layer deposition SiO_2 using plasma treatment cycle, J. Vac. Sci. Technol. A 33 (2015) 01A146.
[49] S.B. Jin, Y.J. Kim, Y.S. Choi, I.S. Choi, J.G. Han, Characterization of silicon oxide gas barrier films with controlling to the ion current density (ion flux) by plasma enhanced chemical vapor deposition, Thin Solid Films 518 (2010) 6385–6389.
[50] D. Apelian, D. Wei, M. Paliwal, Particle-plasma interactions during low pressure plasma deposition, Thin Solid Films 118 (1984) 407.
[51] J. Perrin, Plasma and surface reactions during a-Si: H film growth, J. Non-Cryst. Solids 137 (1991) 639–644.
[52] D. Hegemann, E. K€orner, N. Blanchard, M. Drabik, S. Guimond, Densification of functional plasma polymers by momentum transfer during film growth, Appl. Phys. Lett. 101 (2012) 211603.
[53] E. Gusev, Defects in High-κ Gate Dielectric Stacks, Springer, 2006.
[54] M. Ritala, K. Kukli, A. Rahtu, P.I. Raisanen, M. Leskela, T. Sajavaara, J. Keinonen, Atomic layer deposition of oxide thin films with metal alkoxides as oxygen sources, Science 288 (2000) 319.
[55] P. Boyle, A. Ellingboe, M. Turner, Independent control of ion current and ion impact energy onto electrodes in dual frequency plasma devices, J. Phys. D: Appl. Phys. 37 (2004) 697.
[56] H.C.M. Knoops, E. Langereis, M.C.M. van de Sanden, W.M.M. Kessels, Conformality of plasma-assisted ALD: physical processes and modeling, J. Electrochem. Soc. 157 (2010) G241.
[57] J. Dendooven, D. Deduytsche, J. Musschoot, R. Vanmeirhaeghe, C. Detavernier, Conformality of Al_2O_3 and AlN deposited by plasma-enhanced atomic layer deposition, J. Electrochem. Soc. 157 (2010) G111.
[58] O. Renault, L.G. Gosset, D. Rouchon, A. Ermolieff, Angle-resolved x-ray photoelectron spectroscopy of ultrathin Al_2O_3 films grown by atomic layer deposition, J. Vac. Sci. Technol. A 20 (2002) 1867.
[59] P. Broqvist, A. Pasquarello, Oxygen vacancy in monoclinic HfO_2: a consistent interpretation of trap assisted conduction, direct electron injection, and optical absorption experiments, Appl. Phys. Lett. 89 (2006) 262904.
[60] H. Choi, S. Lee, H. Jung, S. Shin, G. Ham, H. Seo, H. Jeon, Moisture barrier properties of Al_2O_3 films deposited by remote plasma atomic layer deposition at low temperatures, Jpn. J. Appl. Phys. 52 (2013) 035502.
[61] W.-S. Kim, M.-G. Ko, T.-S. Kim, S.-K. Park, Y.-K. Moon, S.-H. Lee, J.-G. Park, J.-W. Park, Titanium dioxide thin films deposited by plasma enhanced atomic layer deposition for OLED passivation, J. Nanosci. Nanotechnol. 8 (2008) 4726.